MATEC Web of Conferences **14**, 05001 (2014)
DOI: 10.1051/matecconf/20141405001

Microstructural damage evolution in two Ni based superalloys subjected to different mechanical loading conditions through quantitative EBSD measurements using Cross-Court software

E. Vacchieri[1,2,a], A. Costa[1], S. Parodi[3], and S.R. Holdsworth[2]

[1] Ansaldo Energia S.p.A., Corso Perrone 118, 16161 Genoa, Italy
[2] EMPA, Überlandstrasse 129, 8600 Dübendorf, Switzerland
[3] Department of Chemistry, University of Genoa, Via Dodecaneso 31, 16146 Genoa, Italy

Abstract. Ni based superalloys are adopted as base materials for critical hot gas path components of gas turbines. Knowledge of the evolution of the microstructure is very important for gas turbine producers in order for them to fully predict component behaviour in service. Quantitative EBSD measurements have been performed to evaluate the local strain condition of the material after test on creep and LCF testpieces of two Ni based superalloys. The Cross-Court software has been used to quantitatively analyse EBSD patterns by means of the cross-correlation method developed by Wilkinson et al. The results of the quantitative analyses enable microstructural characterisation to be completed and the mechanisms that describe material property evolution to be better understood. In addition some measurements have been extended to real components after service and the results have been correlated to FE simulations.

1. Introduction

Ni based superalloys are used as structural materials for critical components in aero and industrial gas turbines because of their high resistance to deformation. The life of hot gas path blades and vanes is determined by the interaction of creep and fatigue damage because nowadays gas turbine operating profiles require high flexibility, meaning frequent shut-down/start-up cycles. The gas turbine producers should know the materials behaviour in this kind of operating regime, also in terms of microstructural damage evolution. This knowledge is fundamental to understanding the mechanisms that determine the formation of physical damage and can be exploited to recognise the different damaging phenomena in ex-service material.

Ni based superalloys are characterised by a composite microstructure, composed of an austenitic γ matrix, strengthened by solid solution elemental substitution, and a high volume fraction γ' phase precipitate distribution (50–70%, depending on the composition of the alloy). The peculiarity of these precipitates is that they are intermetallic phase Ni_3Al, with an ordinate structure, and coherent with the γ matrix. The physical metallurgy of superalloys is strictly related to their microstructure, and its stability at high temperature under the application of mechanical and thermal loading accounts for the outstanding performance of these materials in service [1,2].

Electron backscatter diffraction (EBSD) is considered an alternative laboratory-based technique and is a key materials characterization tool with widespread availability, helping to understand microstructure–property relationships in numerous materials. In the last years, Wilkinson et al. [3–5] have developed the cross-correlation-based analysis of EBSD patterns. The high angular resolution electron backscatter diffraction (HR-EBSD) technique allows measurements of elastic strain (i.e. stress) and lattice misorientations with high sensitivity ($<10^{-4}$ strain, $<10^{-4}$ rads/0.006° rotation [4, 5]). HR-EBSD probes the strain state of the lattice while capturing information characterising the local microstructural environment, and so bridges the gap between smaller length scale transmission electron microscope (TEM) investigations and volume-averaging x-ray and neutron methods [6].

In the present paper, cross-correlation-based analysis has been conducted using the commercial Cross-Court software package [7] on results for the two Ni based superalloys, one equiaxed and one single crystal, in the as delivered conditions and after mechanical tests in order to correlate internal strain, stress and dislocation density measurements with mechanical properties. Finally, the cross-correlation analysis has been extended to ex-service materials and the results have been compared with FE simulation predictions.

2. Experimental procedures

2.1. Materials

The first alloy is the polycrystalline Ni based superalloy, René 80, which is characterised in the fully heat treated condition by a bimodal distribution of γ' phase, as depicted

[a] Corresponding author: erica.vacchieri@aen.ansaldo.it

Table 1. Chemical composition (wt%) of the two superalloys.

	Wt%										
Element	Ni	Cr	Co	Al	Ti	W	Mo	Ta	C	Zr	B
René 80	Bal	14.0	9.50	3.00	5.00	4.00	4.00	-	0.17	0.05	0.02
PWA1483SX	Bal	12.2	9.00	3.60	4.08	3.80	1.90	5.00	0.07	-	-

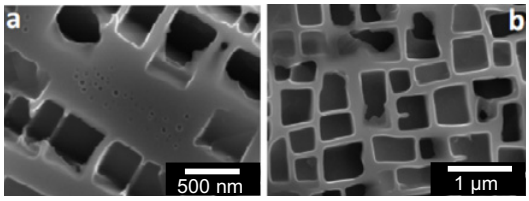

Figure 1. SEM micrograph of the as delivered γ/γ' microstructure of (a) René 80 and (b) PWA1483SX.

in Fig.1a. The primary γ' phase particles are cuboidal and their equivalent side is about 400 nm. Secondary γ' phase precipitates in γ channels during ageing heat treatment in spheroidal shape as particles which are smaller than 20 nm. The total γ' volume fraction for this alloy is typically 50%.

The second material is a first generation SX superalloy, PWA1483SX, whose microstructure is characterised by a monomodal distribution of γ' phase. In the fully heat treated condition this alloy shows cuboidal γ' phase particles, about 500 nm in equivalent size and about 60% volume fraction. The starting microstructure is reported in Fig. 1b.

The compositions of the two alloys are displayed in Table 1.

2.2. Mechanical testing

Mechanical test specimens were machined from investment cast test bars for both the alloys. For SX material the test bars were solidified in a nominal ⟨001⟩ orientation, with an acceptance limit on θ as set for actual components. All the specimens were tested in the fully heat treated condition.

An extensive mechanical testing campaign was performed in the last years to characterise the behaviour of these two materials, completed by a comprehensive microstructural evaluation of samples after test. In this paper the results of the microstructural characterisation are completed by EBSD quantitative measurements conducted on creep and low cycle fatigue (LCF) specimens after test. In particular for creep, failed and interrupted tests have been examined for both alloys. For René 80, the analysed creep tests have been conducted at 800 °C and 950 °C. The same load condition at the same testing temperature was applied on two samples, one stopped after 1% elongation was reached and the other one stopped after failure. For the single crystal superalloy, the creep test temperatures were 900 °C, 950 °C and 1000 °C and the interruption elongation was 2%. LCF tests for both the materials were performed in strain control with a triangular wave, R $(\varepsilon_{min}/\varepsilon_{max}) - 1$ and a constant strain rate of 10^{-2} s^{-1}. The selected test temperatures for René 80 were 400 °C, 800 °C and 900 °C, while for the SX alloy they were 700 °C, 850 °C and 950 °C. For each testing temperature three strain levels were chosen for both materials (from 0.5% to 1.7%, depending on the temperature value). All the samples were analysed after the failure criteria was reached (20% load drop).

2.3. Microstructural characterisation and EBSD analysis methodology

The damage condition was established through microstructural investigations on the samples after test.

Longitudinal sections of the specimens were analysed using classical fractographic and metallographic instruments and more advanced characterization techniques. γ' phase features and γ/γ' interfacial dislocations were studied by FEG-SEM SE and In-Beam detector [8,9] after selective metallographic etching for γ' phase ($HF+MoO_3$ reagent). Classical EBSD analyses have been performed in the same regions where γ' phase was characterised on the sample longitudinal sections. Moreover HR-EBSD patterns (1×1 binning) have been collected in the same locations and analysed with Cross-Court [7]. For EBSD mapping, the samples were multiple polish/etched with an extra final polishing stage with colloidal SiO_2.

Cross-Court software analysed the EBSD patterns comparing each one to a reference pattern through cross-correlation functions calculated via a Fourier domain [4]. The difference in zone axis position is evaluated through a displacement gradient tensor **A** that can be decomposed into elastic strain and lattice rotation [10]. The reference pattern is from the same mapped region and is selected by the operator, ideally from a strain-free region or from a point on the sample for which the strain is known. However it was not possible for the analysed testpieces as the mapped regions were inside the gauge lengths of the mechanically tested samples. Even when the reference pattern comes from a region with unknown strain, important information (lattice curvatures and elastic strain gradients) can still be determined and used to recover the GND (geometrically necessary dislocation) density distribution [11]. The GND density has been evaluated utilising the analysis given by Nye [12] and the assumptions for FCC crystals made by J. Jiang et al. [13] have been here considered. The GND are considered the most important to determine plastic strain as they are to a first approximation independent of the material but strictly related to the microstructure, that means the geometric arrangement and size of grains and phases [14]. For René 80 samples, each region of the gauge length was characterised by three maps (Fig. 2): map 1 to capture patterns from more than one grain (area $570 \times 570\,\mu m^2$, step size $7\,\mu m$), map 2 and 3 inside a single grain (area $170 \times 170\,\mu m^2$, step size $2\,\mu m$). For PWA1483SX, as it is single crystal, only the higher magnification map has been

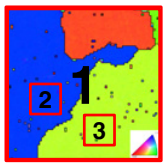

Figure 2. EBSD maps on René 80 samples – (1) 570 × 570 μm^2 multi-grain map and (2) and (3) 170 × 170 μm^2 single crystals maps.

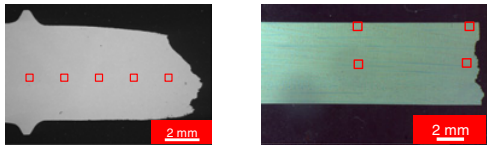

(a) (b)

Figure 3. EBSD analysed regions (red boxes) in the longitudinal section of the (a) creep sample and (b) fatigue specimen.

collected for each analysed region. The step sizes for the two different magnifications have been chosen in order to collect a sufficient quantity of data points in a reasonable time. The high magnification was chosen to be not too high in order to not resolve the γ/γ' phase microstructure but to be representative of a "mean" microstructure. In fact, in Ni based superalloys the dislocations develop mainly in the γ matrix [1,2], but, due to the high volume fraction and small sizes of γ' phase particles, it is difficult to discriminate between these phases. Moreover, the high magnification map conditions are the same for both the materials and a comparison of the collected results can be performed.

Creep samples were analysed in five regions from the shoulder to the fracture surface or within the gauge length for interrupted tests, as shown in Fig. 3a. LCF specimens were studied in four regions, two close to the external surface and two in the centre of the metallographic section, at different depths with respect to the fracture surface, as depicted in Fig. 3b. For ex-service components the same analysis strategy has been applied for the two different materials. The critical locations, where cracks were observed, have been studied and compared to laboratory tested materials. The output of the Cross-Court analyses that have been considered to compare material condition after different mechanical test and after service is a series of GND density maps.

With respect to already published studies on structural materials [11,15,16] the approach defined here is relatively coarse, but extended to a huge number of specimens tested in different conditions. Importantly, it allows in an industrial organisation to develop further knowledge on material damage evolution and to assess a tool that can be applied to evaluate material condition on ex-service components.

3. Results and discussion

The HR-EBSD measurements determined by means of the cross-correlation method are here shown and discussed, while the other aspects of the microstructural evolution are only briefly reported for comparison with the damage evaluation through Cross-Court software. A comprehensive review on the microstructural evolution for these alloys can be found in [17].

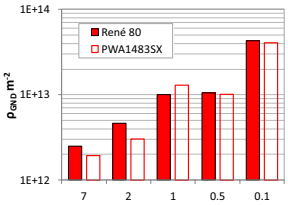

Figure 4. GND density (ρ_{GND}) in the as delivered samples for René 80 (shaded columns) and PWA1483SX (unshaded columns), measured by different step sizes, from 7 μm to 0.1 μm.

3.1. As delivered condition

A preliminary activity has been completed on as delivered samples in order to set up the EBSD analysis strategy and to determine their starting conditions.

As suggested in [11,13] the quality of the maps has been checked by looking at the values for the mean angular error (MAE) and the geometric mean of XCF (cross-correlation function) peak height (PH), and thresholds of PH>0.2 and MAE<0.008 rad values have been selected [13]. It was not possible to apply these thresholds to all the observations from all the maps, in particular for ex-service materials, but the MAE and PH maps have been used to provide the basis of comments on the results.

To check the effect of step size on mean values of GND density for the as delivered samples, five step sizes have been used to collect EBSD maps (all with the same total number of collected patterns) and the results are shown in Fig. 4. Later on, only the high magnification areas with 2 μm step size (170 × 170 μm^2) have been quantitatively analysed to compare the samples after different testing conditions. The GND densities show an increase of their mean value with a decrease of the step size and this behaviour has also been observed by J. Jiang et al. [13] on deformed polycrystalline Cu. As the HR-EBSPs have been collected and analysed the variation in GND density cannot be related to the noise but to the change in separation between statistically stored dislocations (SSDs) and GNDs due to the change in Burger circuit size [13]. The choice of 2 μm step size maps is strictly related to the need of a "mean" γ/γ' information and of a significant amount of data from a not too small area without increasing the number of maps per sample.

3.2. Creep damage

In Fig. 5, an example of γ' phase features, standard EBSD GROD (grain reference orientation deviation maps) and GND density maps along the gauge length of a creep sample after failure are shown for the SX alloy. The γ' phase shows the presence of rafting and appears wavy and irregular in the whole gauge length; EBSD maps highlight the loss of coherence between γ and γ' phase in the region towards the fracture surface. The GND density increases towards the fracture surface; in this region the quality of the maps decreases and a significant amount of

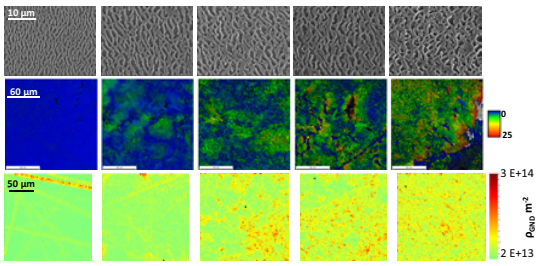

Figure 5. PWA1483SX – SEM-SE γ' phase microstructure, IQ+GROD maps and GND density maps along the gauge length from the shoulder (first left) to the fracture surface (last right) in the sample after failure tested at 950 °C and 130MPa.

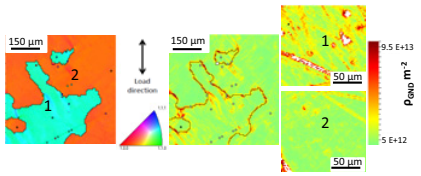

Figure 6. René 80 – Inverse Pole Figure (IPF) and GND density map at low magnification and on two different oriented grains at high magnification in the middle of the gauge length of a crept sample until failure, tested at 950 °C and 130 MPa.

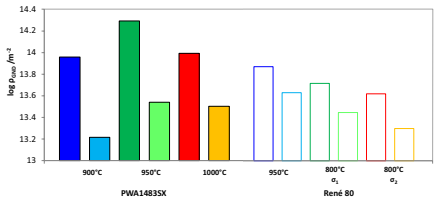

Figure 7. Mean GND density measured in the gauge length of the analysed sample for PWA1483SX tested at 900°, 950° and 1000 °C and for René 80 tested at 800 °C with two different loads ($\sigma_1 > \sigma_2$) and at 950 °C.

experimental points are outside the threshold values for PH and MEA. The interrupted sample, tested in the same condition, shows a more homogeneous rafted γ' phase and standard and Cross-Court EBSD maps depict a more uniform condition. The highest GND density mean value is observed in the centre of the gauge length.

René 80 creep samples do not show for all the testing conditions the rafting of γ' phase, as the testing temperature is too low, below 850 °C [17], and the stress is too high to be in the rafting regime [1]. The EBSD maps in this testing condition do not highlight the loss of coherence between γ and γ' phase but they show the presence of micro-twinning, due to the low temperature creep mechanism for this class of alloys [2, 17].

The GND density maps at low magnification highlight the localisation of the highest values close to the grain boundaries, as expected. Also for this alloy, the GND density maps at high magnification show an increase of the mean value towards the fracture surface for the failed samples and a relative maximum in the centre of the gauge length for the interrupted specimens. For each region two different grains have been studied and the results can be different as their relative orientation with respect to the loading direction changes, Fig. 6. In fact, each grain in

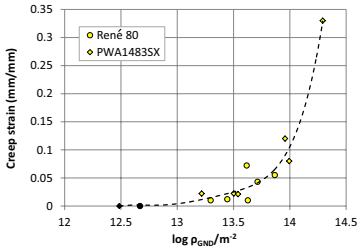

Figure 8. Mean GND density values for all the analysed samples versus creep strain measured at the end of the test for PWA1483SX (diamonds) and René 80 (circles).

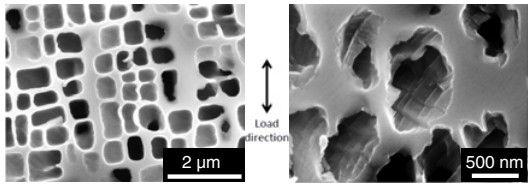

Figure 9. FEG-SEM In-Lens micrographs of γ/γ' phase interfacial dislocations in the gauge length of (a) PWA1483SX LCF sample tested at 950 °C 1% strain range and (b) René 80 LCF sample tested at 900 °C 1% strain range.

a polycrystalline material deforms by a different amount, depending on its orientation and the constraints imposed on it by its neighbours [14].

A comparison between GND density mean values as a function of the testing condition for the two alloys is summarised in Fig. 7. The SX alloy shows higher values for the failed samples with respect to the failed René 80 coupons that show a smaller difference in the GND density mean value with respect to the interrupted samples. This is due to the higher failure creep strain that SX reaches because of its higher ductility with respect to René 80.

The GND densities measured along the gauge length of each sample have been averaged and the mean values have been compared to the creep strain reached at the end of the creep tests for each specimen of the two alloys. In Fig. 8 the GND densities correlate with the creep strain, following the same polynomial curve for both materials. The reason why the solidification macrostructure has no effect is mainly due to the fact that the values have been obtained from high magnification maps that come from inside distinct grains and so it does not take into account of the grain boundary role in damage evolution. In fact, in particular for René 80, the scatter is high as the measurement points come from a higher number of measurements from different oriented grains. However, the unique correlation between GND density and creep strain is a very interesting result that can be exploited for the evaluation of material after service, trying to correlate measured GND density to local plastic strain.

3.3. Fatigue damage

The γ/γ' phase microstructure after LCF test is not highly modified in terms of geometrical features while a modification of the interfacial dislocation patterns (Fig. 9) is observable for both the alloys.

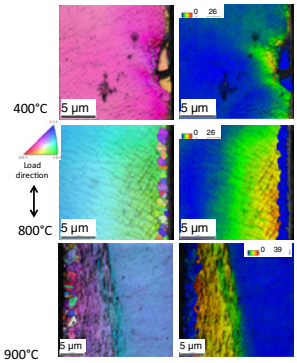

Figure 10. René 80 – standard EBSD maps (IPF+IQ and GROD+) under the external surface in the middle of the gauge length of the metallographic section of LCF samples that show the deformed region and the presence of a recrystallised layer for the higher temperatures.

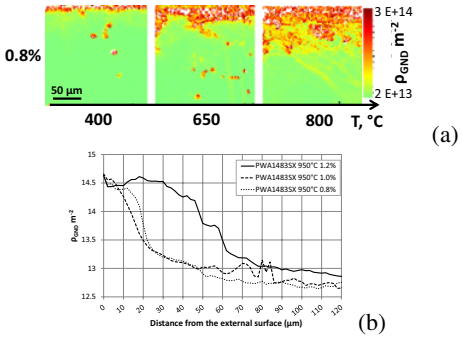

Figure 11. (a) GND density map on the external surface in the middle of the gauge length of René 80 LCF samples; (b) GND density profile from external surface towards sample centre for PWA1483SX LCF samples tested at 950 °C with different $\Delta\varepsilon$.

A significant modification of the γ/γ' phase microstructure happens only in the regions close to the external and fracture surfaces. In these regions the deformation is localised and it reaches a significant plastic contribution with respect to the total plastic strain, evaluated from the σ/ε hysteresis loop data. The localisation of the damage has been confirmed by standard EBSD maps that highlight the presence of a recrystallized layer for the highest test temperatures, Fig. 10. The Cross-Court measurements in these regions allow the evaluation of the reached values of GND density and their trend from external surface towards internal parts of the sample sections, as shown in Fig. 11. As for the creep samples, the presence of different oriented grains can mean for René 80 a slightly different absolute GND density.

The mean GND density values obtained from a thin layer close to the external surface have been calculated for both the materials and a threshold value, for which failure of the sample happens, has been identified for the two alloys (Fig. 12). The threshold values are very similar for the two materials ($log(\rho_{GND})$ 14.38 for René 80 and 14.47 for SX).

The sample core GND density measurements have been correlated to the inelastic strain measured from σ/ε hysteresis loop mechanical test data. This correlation is

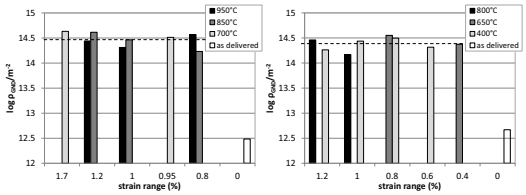

Figure 12. Mean GND density values from the deformed layer under external surface for (a) PWA1483SX and (b) René 80, as a function of the applied strain range for all the analysed samples, and comparison to as delivered condition.

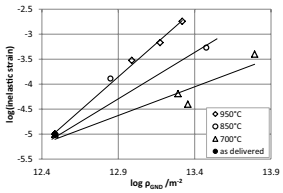

Figure 13. PWA1483SX – Sample core GND density values for LCF samples as a function of inelastic strain evaluated from mid-life cycle hysteresis loop.

not satisfying as a huge scatter, in particular for René 80, is found without a clear correlation to the measured strain data from mechanical responses of the materials. In particular, the mean GND densities for René 80 in the centre of the gauge length are bigger than PWA1483SX, unlike to what has been observed for the region close to the external surface, where the two alloys show very similar values. The GND densities from the core of fatigue samples for both the materials are in the same order of magnitude of creep specimen values even if their macroscopic inelastic strain is 2–3 orders of magnitude lower than creep strain. The higher GND density values in the fatigue samples can be ascribed to the hardening due to cyclic plasticity [14] that is more evident for the lower temperature for both alloys, as shown in Fig. 13.

3.4. Ex-service components

The Cross-Court measurements have been extended to ex-service materials, looking at the critical locations where cracks are observed. In Fig. 14 the SX operated material conditions are shown in terms of crack and γ' phase features. The red squares, in Fig. 14, highlight the regions where Cross-Court measurements have been conducted. The results are reported in Fig. 16: the regions close to the crack show highest GND density values.

Three different components, that withstand to different operative profile, from base load to daily cycling, have been analysed in the same region and the mean GND values have been compared (Fig. 16). An additional very interesting result is that the GND density increases with the increase of start-up/shut-down cycle number. The measured values in operated material are similar to the GND values measured on PWA1483SX interrupted creep samples (see Fig. 9).

A similar procedure has been applied on René 80 operated components. In this case two critical locations

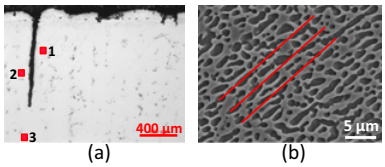

Figure 14. PWA1483SX – (a) OM micrographs of the selected critical location on operated component in SX alloy and (b) SEM-SE γ' phase microstructure in the region close to the crack.

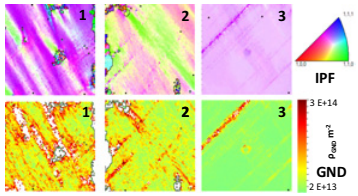

Figure 15. PWA1483SX – IPF and GND density maps for the three locations highlighted by red squares in Fig. 15.

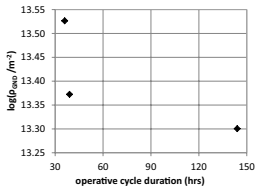

Figure 16. PWA1483SX – Mean GND density values measured on critical location of operated components as a function of the operative cycle duration.

in the same part have been considered. The difference between the two locations is the features of the cracks, intergranular for location (a) and mixed propagation mode for location (b), and the output of FE simulation, as shown in Fig. 17.

The results, reported in Fig. 18, show that between the two analysed regions the most critical is the location (a) rather than location (b) as expected from the crack lengths and FE simulations. Moreover, between the two examined components with different operating regimes, the highest values have been measured in both the locations of the daily cycled component.

The observed GND densities in operated components are close to the threshold value identified for René 80 in fatigue samples in the region close to the external surface.

4. Conclusions

The Cross-Court software has been applied to HR-EBSD maps collected on two Ni based superalloys in the as delivered condition and after creep and LCF mechanical tests. The obtained results can be summarised as follow:

- the Cross-Court output is strictly related to the conditions of EBSD map acquisition.
- Creep damage evolution in sample gauge length has been confirmed quantitatively through GND density. The mean GND density values in each sample gauge length have been correlated to creep strain reached at the end of the test and a unique relationship has been identified for the two materials.

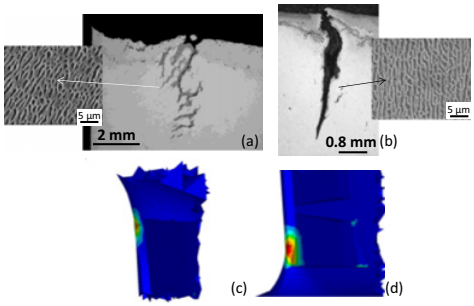

Figure 17. René 80 – (a) and (b) OM micrographs of the two critical locations and (c) and (d) corresponding creep strain obtained from FE simulation.

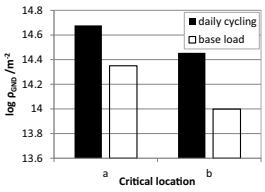

Figure 18. René 80 – GND density mean values of the two critical locations for two components characterised by different operative profiles.

- Fatigue damage is similar in the two materials as it localises at the external and fracture surface, where a similar threshold value of GND density has been identified.
- The developed strategy has been applied to operated material for the two alloys and it has been possible to correlate the GND density to the increase in start-up/shut-down cycle number.

References

[1] R.C. Reed, *The superalloys* (Cambridge Univ. Press, Cambridge, 2006)
[2] H. Mughrabi, Mat. Sci. Technol. **25**, 2 (2009) 191–204
[3] A.J. Wilkinson, Ultramicroscopy **62** (1996)
[4] A.J. Wilkinson, et al., Ultramicroscopy **106** (2006) 307–313
[5] A.J. Wilkinson, et al., Mater. Sci. Technol. **22** (2006) 1271–1278
[6] T. B. Britton, et al., JOM **65**, 9 (2013) 1245–1253
[7] www.blgproductions.co.uk
[8] A. Epishin, J. Microscopy **228**, 2 (2007) 110–117
[9] L. Dirand, et al., Mat. Charact. **77** (2013) 32–46
[10] T.B. Britton, et al., Ultramicroscopy **114** (2012) 82–95
[11] A.J. Wilkinson, et al., J. Strain Analysis Eng Design **45** (2010) 365–376
[12] J.Nye, Acta Metal. **1** (1953) 153
[13] J. Jiang, et al., Ultramicroscopy **125** (2013) 1–9
[14] M.F. Ashby, Phil. Mag. **21**:170 (1970), 399–424
[15] Dong HE, et al., Trans. Nonferrous Met. Soc. China **23** (2013) 7–13
[16] P. Villechaise, et al., Superalloys 2012 (2012) 15–24
[17] E. Vacchieri, A. Costa, Superalloys 2012 (2012) 235–244